**Supporting Information**

# Fundamental properties of TEMPO-based catholytes for aqueous redox flow batteries: effects of substituent groups and electrolytes on electrochemical properties, solubilities and battery performance

Wenbo Zhou,[a] Wenjie Liu,[a] Meng Qin,[a] Zhidong Chen,[a] Juan Xu, *[a] Jianyu Cao *[a] and Jun Li *[b]

[a]*Jiangsu Key Laboratory of Advanced Catalytic Materials and Technology, Changzhou University, Changzhou 213164, China.*

[b]*School of Intelligent Systems Engineering, Sun Yat-Sen University, Shenzhen 518000, China. lijun255@mail.sysu.edu.cn (J. Li)*

*Corresponding author,

E-mail: jycao@cczu.edu.cn (J. Cao); cjytion@cczu.edu.cn (J. Xu); lijun255@mail.sysu.edu.cn (J. Li)

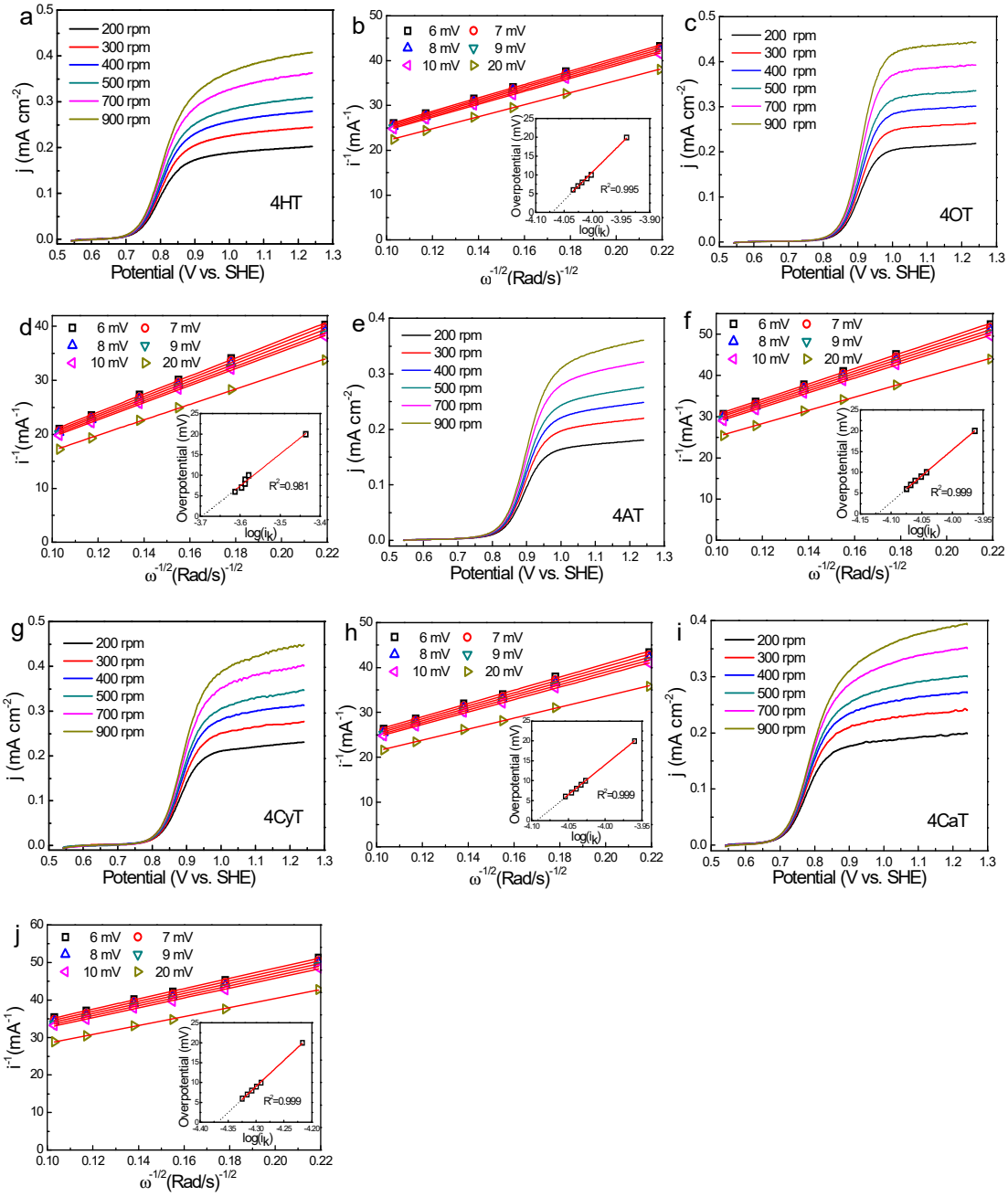


**Fig. S1** RDE voltammetry curves of 1 mM 4HT (a), 4OT (b), 4AT (c), 4CyT (d) and 4CaT (e), respectively, in 0.5 M KCl at 6 rotation rates ranging from 200 to 900 rpm. (b, d, f, h and j) Koutecky-Levich plots derived from these RDE data at different oxidation overpotentials. The insets of (b, d, f, h and j) are the fitted curves of Butler-Volmer equation using the kinetic current density ($j_k$) obtained from the zero-intercept of Koutecky-Levich plots in (b, d, f, h and j) at six different oxidation overpotentials.

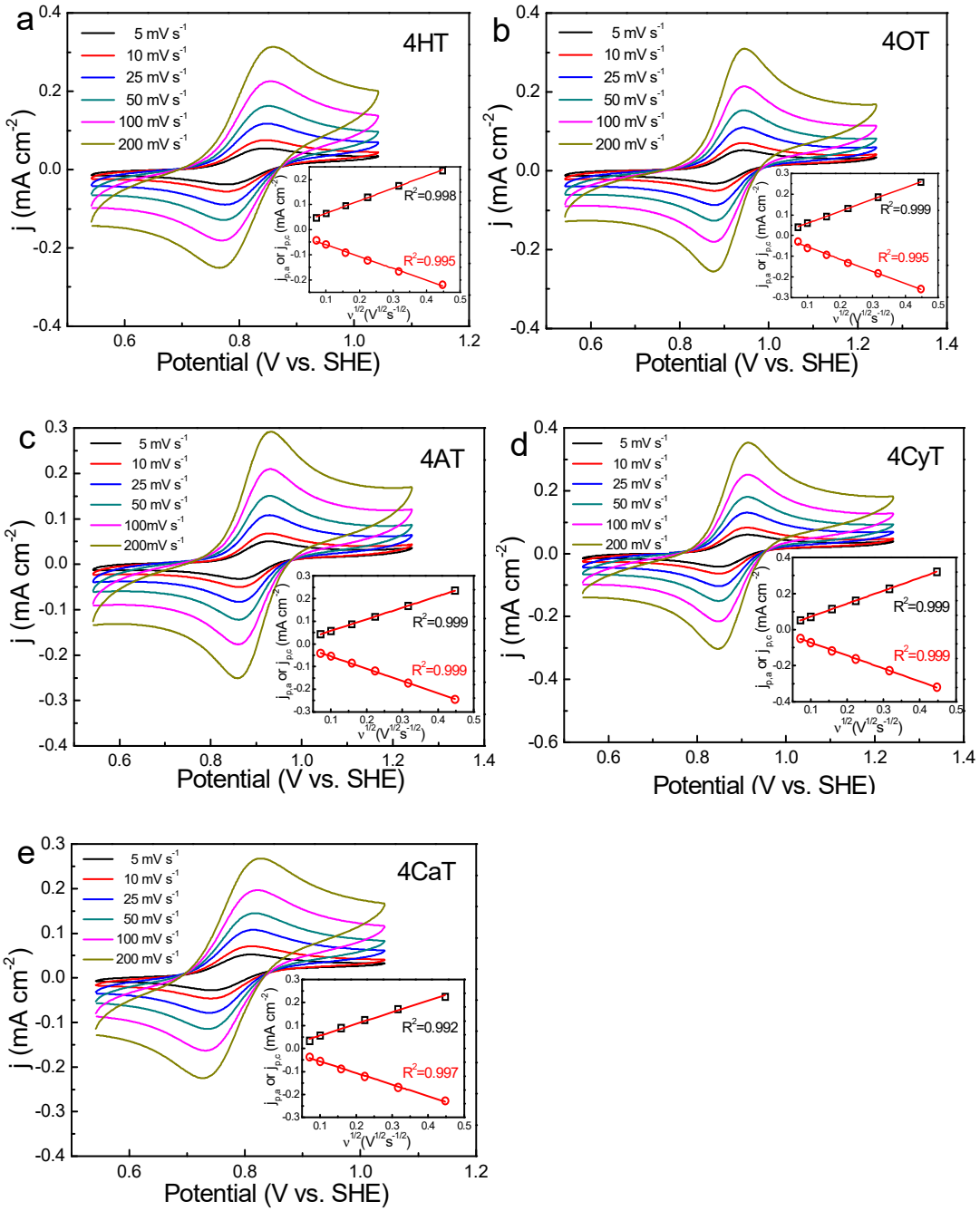


**Fig. S2** CVs of 1 mM 4HT (a), 4OT (b), 4AT (c), 4CyT (d) and 4CaT (e), respectively, in 0.5 M KCl solution at different scan rates. The insets of (a-e) are the plots of the oxidation and reduction peak current density ($j_{p,a}$ and $j_{p,c}$) versus square root of the scan rates ($v^{1/2}$).

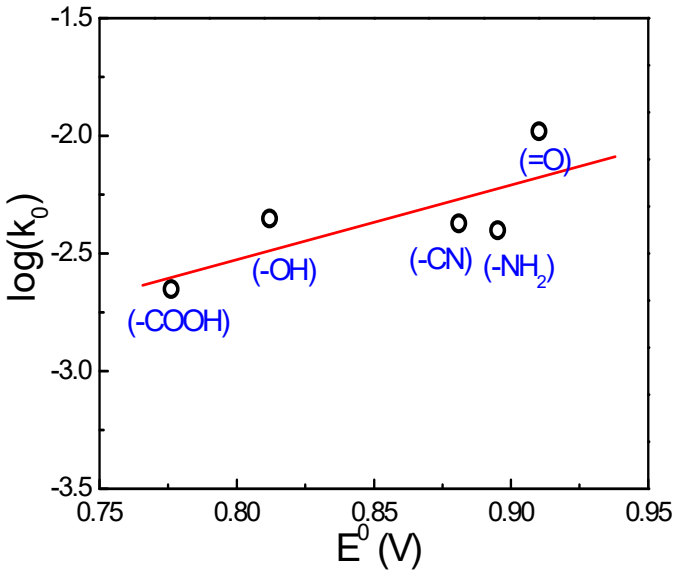


**Fig. S3** Plot of the logarithm of the rate constant versus the standard potential.

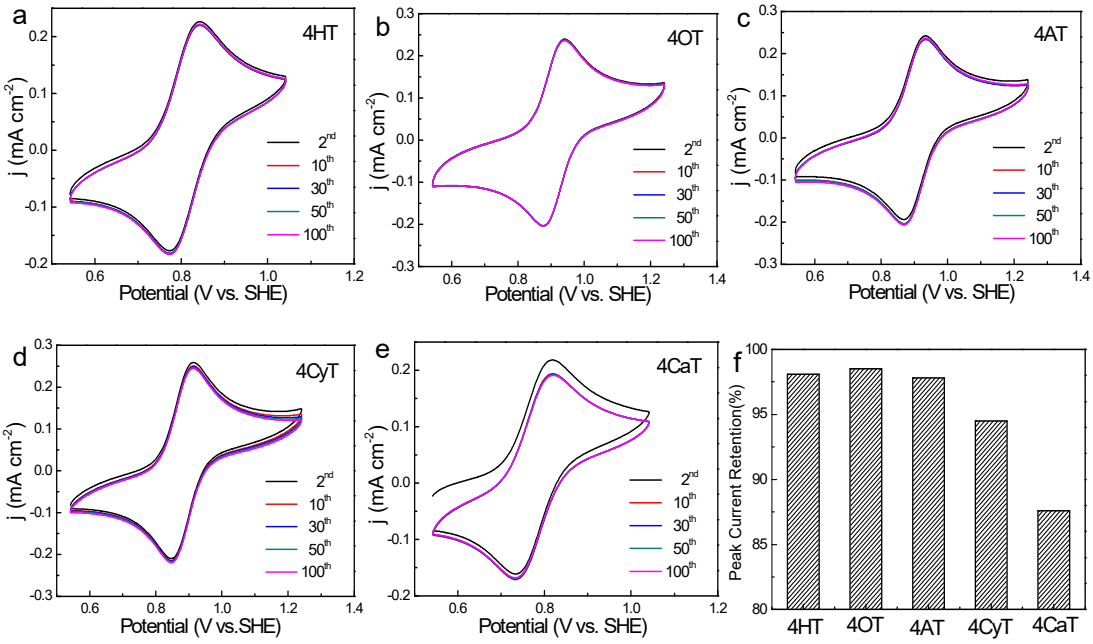


**Fig. S4** CVs of 1 mM 4HT (a), 4OT (b), 4AT (c), 4CyT (d) and 4CaT (e), respectively, in 0.5 M KCl supporting electrolyte at 100 mV $s^{-1}$ during the $2^{nd}$, $10^{th}$, $30^{th}$, $50^{th}$ and $100^{th}$ cycles. (f) Peak current retention histogram obtained from CVs before and after 100 cycles.

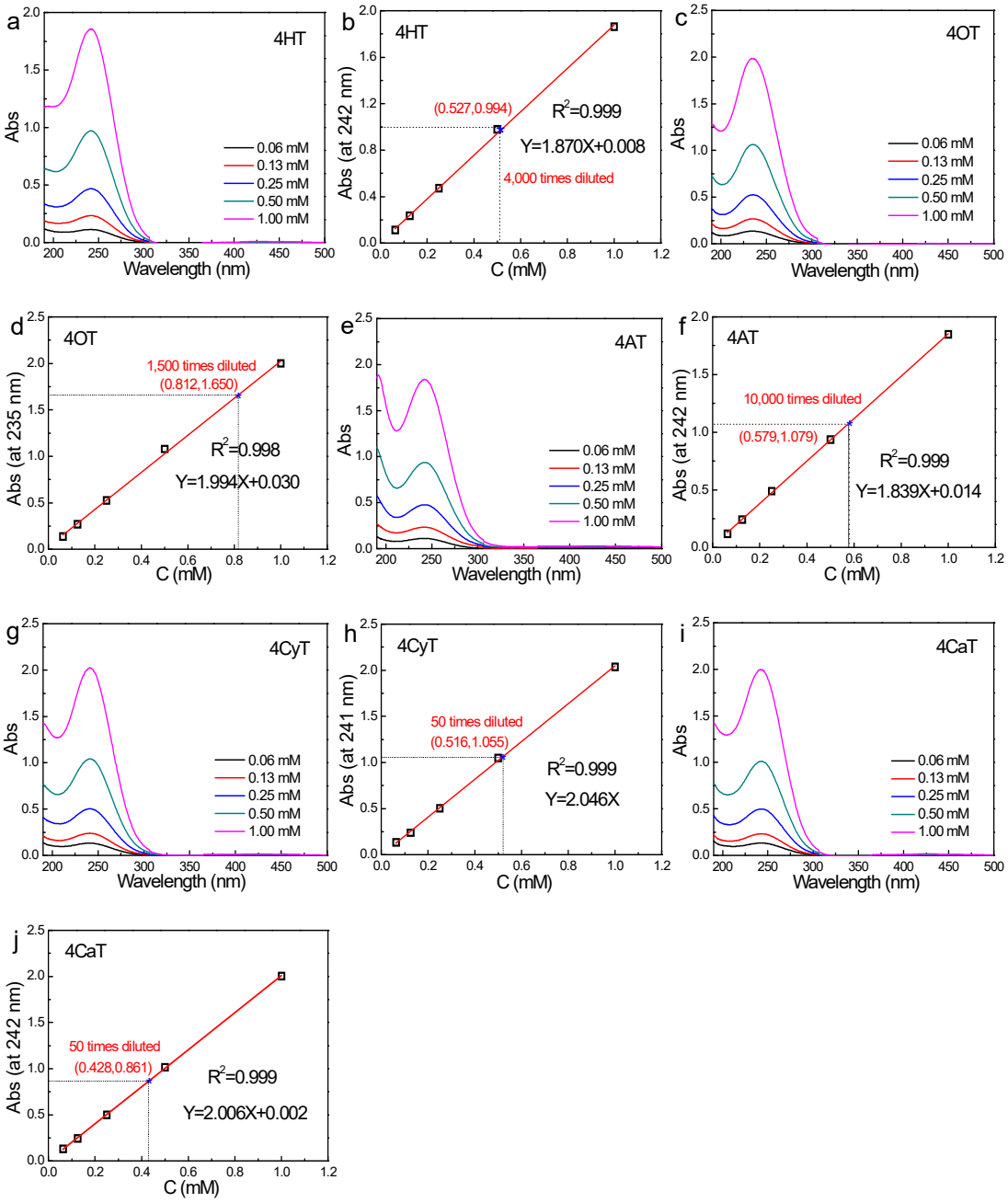


**Fig. S5** UV-vis absorption spectra of 4HT (a), 4OT (c), 4AT (e), 4CyT (g) and 4CaT (i), respectively, in pure water with different concentration. The linear plot between the concentration and the absorbance for 4HT (b), 4OT (d), 4AT (f), 4CyT (h) and 4CaT (j), respectively. The solubilities were summarized in **Table 1**.

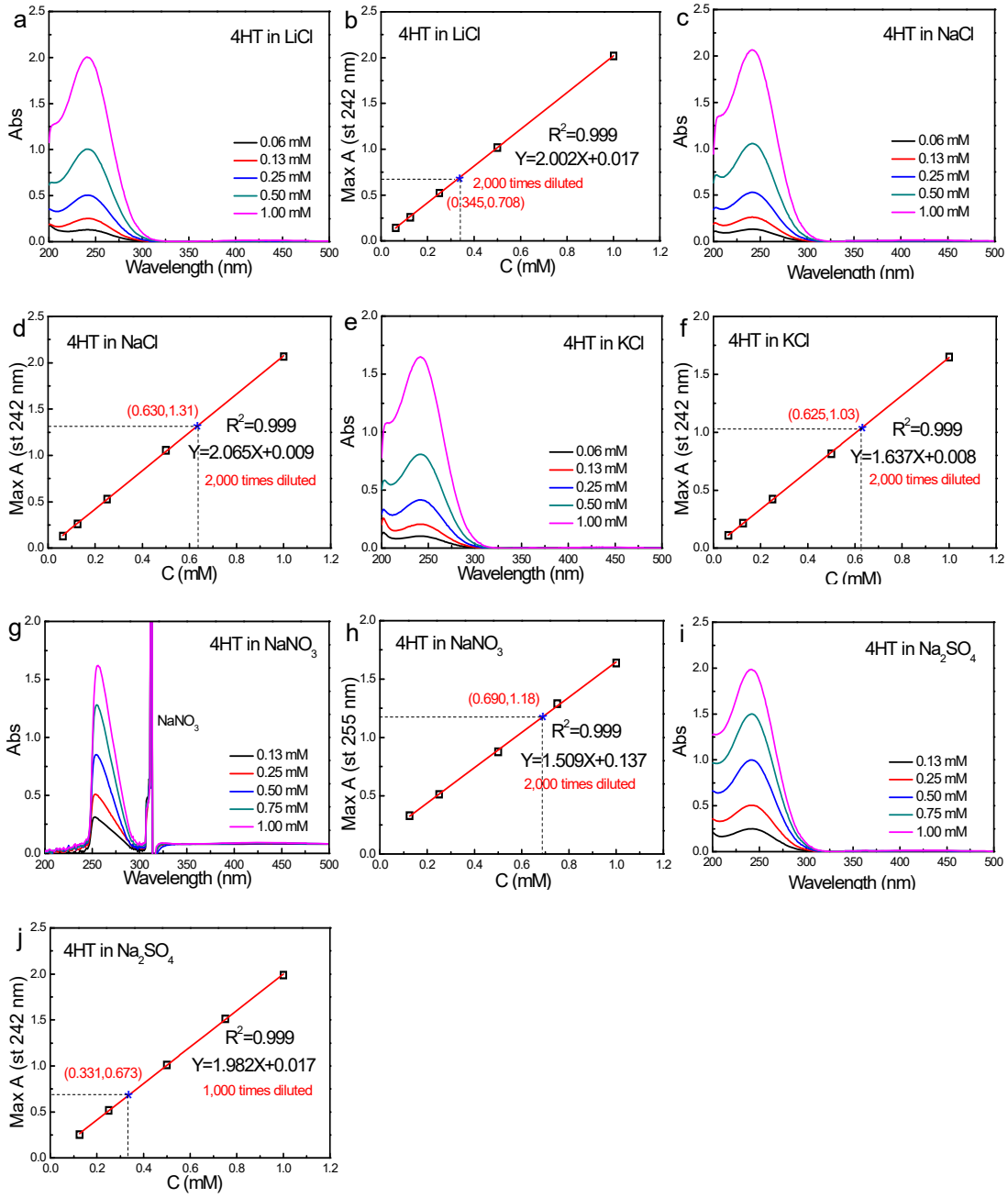


**Fig. S6** UV-vis absorption spectra of 4HT with different concentration in LiCl (a), NaCl (c), KCl (e), $NaNO_3$ (g) and $Na_2SO_4$ (i) aqueous solution, respectively. The concentration of supporting electrolyte is 0.5 M. The linear plot between the concentration of 4HT and the absorbance in LiCl (b), NaCl (d), KCl (f), $NaNO_3$ (h) and $Na_2SO_4$ (j) aqueous solution, respectively.

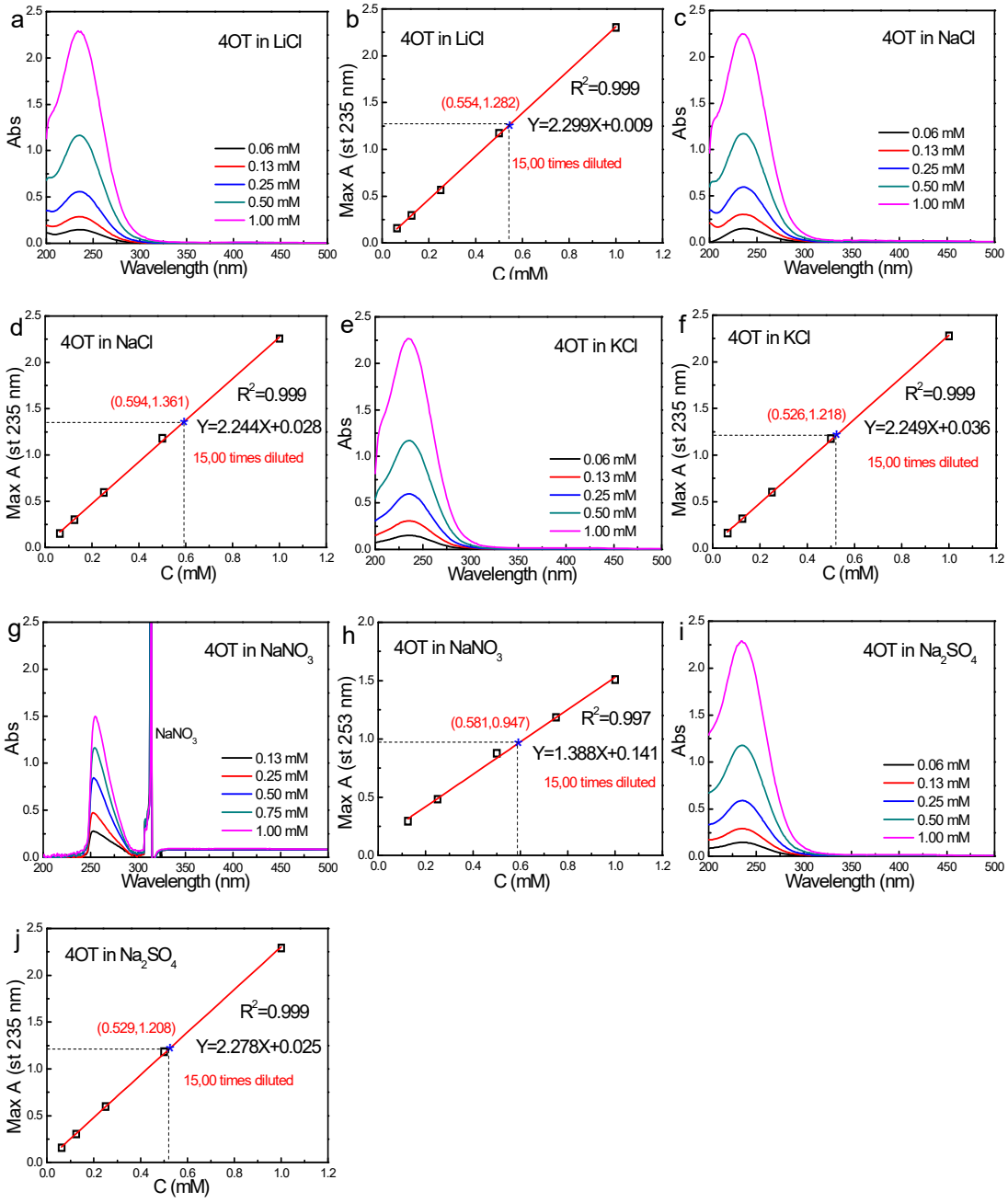


**Fig. S7** UV-vis absorption spectra of 4OT with different concentration in LiCl (a), NaCl (c), KCl (e), $NaNO_3$ (g) and $Na_2SO_4$ (i) aqueous solution, respectively. The concentration of supporting electrolyte is 0.5 M. The linear plot between the concentration of 4OT and the absorbance in LiCl (b), NaCl (d), KCl (f), $NaNO_3$ (h) and $Na_2SO_4$ (j) aqueous solution, respectively.

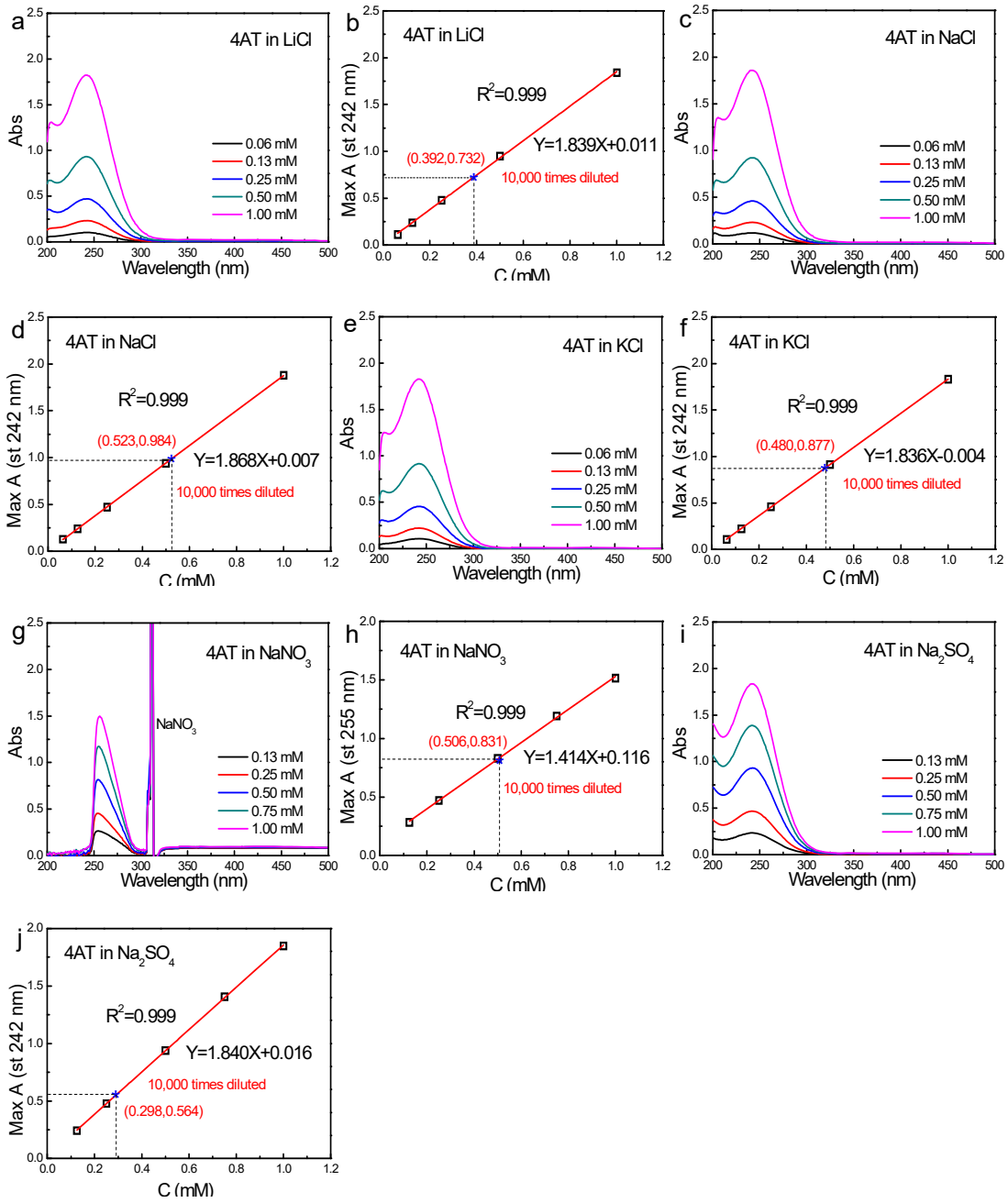


**Fig. S8** UV-vis absorption spectra of 4AT with different concentration in LiCl (a), NaCl (c), KCl (e), $NaNO_3$ (g) and $Na_2SO_4$ (i) aqueous solution, respectively. The concentration of supporting electrolyte is 0.5 M. The linear plot between the concentration of 4AT and the absorbance in LiCl (b), NaCl (d), KCl (f), $NaNO_3$ (h) and $Na_2SO_4$ (j) aqueous solution, respectively.

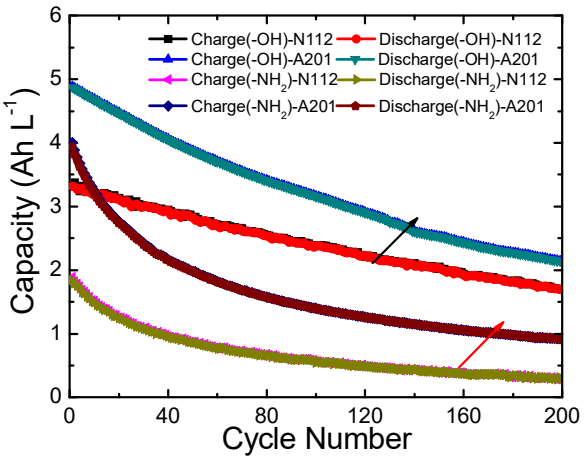


**Fig. S9** Capacity versus cycling numbers for the symmetric RFB at 100 mA $cm^{-2}$. Conditions: anolyte, 0.2 M 4-HO-TEMPO (or 4-$H_2$N-TEMPO) in 2 M KCl aqueous solution; catholyte, 0.2 M oxidation state of 4-HO-TEMPO (or 4-$H_2$N-TEMPO) in 2 M KCl aqueous solution; flow rate, 60 mL $min^{-1}$; separator, A201 IEM.